



submitted to ApJ.

## Higher Order Moments of the Angular Distribution of Galaxies from Early SDSS Data

István Szapudi<sup>1</sup>, Joshua A. Frieman<sup>2,3</sup>, Roman Scoccimarro<sup>11</sup>, Alexander S. Szalay<sup>13</sup>, Andrew J. Connolly<sup>14</sup>, Scott Dodelson<sup>2,3</sup>, Daniel J. Eisenstein<sup>2,4,27</sup>, James E. Gunn<sup>5</sup>, David Johnston<sup>2,3</sup>, Stephen Kent<sup>3</sup>, Jon Loveday<sup>8</sup>, Avery Meiksin<sup>26</sup> Robert C. Nichol<sup>9</sup>, Ryan Scranton<sup>2,3</sup>, Albert Stebbins<sup>3</sup>, Michael S. Vogeley<sup>15</sup>, James Annis<sup>3</sup>, Neta A. Bahcall<sup>5</sup> J. Brinkman<sup>16</sup> István Csabai<sup>17</sup> Mamoru Doi<sup>18</sup>, Masataka Fukugita<sup>18</sup>, Željko Ivezić<sup>5</sup>, Rita S.J. Kim<sup>5</sup>, Gillian R. Knapp<sup>5</sup>, Don Q. Lamb<sup>2</sup>, Brian C. Lee<sup>3</sup>, Robert H. Lupton<sup>5</sup>, Timothy A. McKay<sup>23</sup>, Jeff Munn<sup>24</sup>, John Peoples<sup>3</sup>, Jeff Pier<sup>24</sup>, Constance Rockosi<sup>2</sup>, David Schlegel<sup>5</sup>, Christopher Stoughton<sup>3</sup>, Douglas L. Tucker<sup>3</sup>, Brian Yanny<sup>3</sup>, Donald G. York<sup>2,25</sup>, for the SDSS Collaboration

## ABSTRACT

We present initial results for counts in cells statistics of the angular distribution of galaxies in early data from the Sloan Digital Sky Survey (SDSS). We analyze a rectangular stripe  $2.5^\circ$  wide, covering approximately 160 sq. degrees, containing over  $10^6$  galaxies in the apparent magnitude range  $18 < r' < 22$ , with

---

<sup>1</sup>Institute for Astronomy, University of Hawaii, 2680 Woodlawn Drive, Honolulu, HI 96822, USA

<sup>2</sup>Astronomy and Astrophysics Department, University of Chicago, Chicago, IL 60637, USA

<sup>3</sup>Fermi National Accelerator Laboratory, P.O. Box 500, Batavia, IL 60510, USA

<sup>4</sup>Steward Observatory, University of Arizona, 933 N. Cherry Ave., Tucson, AZ 85721

<sup>5</sup>Princeton University Observatory, Princeton, NJ 08544, USA

<sup>6</sup>Department of Physics, Columbia University, New York, NY 10027, USA

<sup>7</sup>Department of Physics, University of Pennsylvania, Philadelphia, PA 19101, USA

<sup>8</sup>Sussex Astronomy Centre, University of Sussex, Falmer, Brighton BN1 9QJ, UK

<sup>9</sup>Department of Physics, 5000 Forbes Avenue, Carnegie Mellon University, Pittsburgh, PA 15213, USA

<sup>10</sup>Space Telescope Science Institute, Baltimore, MD 21218, USA

<sup>11</sup>Department of Physics, New York University, 4 Washington Place, New York, NY 10003

<sup>13</sup>Department of Physics and Astronomy, The Johns Hopkins University, Baltimore, MD 21218, USA

<sup>14</sup>University of Pittsburgh, Department of Physics and Astronomy, Pittsburgh, PA 15260, USA

<sup>15</sup>Department of Physics, Drexel University, Philadelphia, PA 19104, USA

<sup>16</sup>Apache Point Observatory, P.O. Box 59, Sunspot, NM 88349-0059

<sup>17</sup>Department of Physics of Complex Systems, Eötvös University, Budapest, Hungary, H-1088

<sup>18</sup>University of Tokyo, Institute of Astronomy and Research Center of the Early Universe, School of Science

<sup>19</sup>University of Tokyo, Institute for Cosmic Ray Research, Kashiwa, 2778582

<sup>20</sup>US Naval Observatory, 3450 Massachusetts Ave., NW, Washington, DC 20392-5420

<sup>25</sup>Remote Sensing Division, Naval Research Laboratory, 45555 Overlook Ave. SW, Washington DC 20375

<sup>22</sup>Astronomical Institute, Tohoku University, Aoba, Sendai 980-8578, Japan

<sup>23</sup>University of Michigan, Department of Physics, 500 East University, Ann Arbor, MI, 48109

<sup>24</sup>US Naval Observatory, Flagstaff Station, P.O. Box 1149, Flagstaff, AZ 86002-1149

<sup>25</sup>Enrico Fermi Institute, 5640 South Ellis Avenue, Chicago, 60637

<sup>26</sup>University of Edinburgh, Royal Observatory, Blackford Hill, Edinburgh EH9 3HJ, UK

areas of bad seeing, contamination from bright stars, ghosts, and high galactic extinction masked out. This survey region, which forms part of the SDSS Early Data Release, is the same as that for which two-point angular clustering statistics have recently been computed. The third and fourth moments of the cell counts,  $s_3$  (skewness) and  $s_4$  (kurtosis), constitute the most accurate measurements to date of these quantities (for  $r' < 21$ ) over angular scales  $0.015^\circ - 0.3^\circ$ . They display the approximate hierarchical scaling expected from non-linear structure formation models and are in reasonable agreement with the predictions of  $\Lambda$ -dominated cold dark matter models with galaxy biasing that suppresses higher order correlations at small scales. The results are in general consistent with previous measurements in the APM, EDSGC, and Deeprange surveys. These results suggest that the SDSS imaging data are free of systematics to a high degree and will therefore enable determination of the skewness and kurtosis to 1% and less than 10%, as predicted by Colombi, Szapudi, & Szalay (1998).

## 1. Introduction

In contemporary models of structure formation, initially small density fluctuations are amplified by gravitational instability to form non-linear structures. Within such structures, the baryons undergo additional non-gravitational processing (gas dissipation, star formation, etc), leading eventually to luminous galaxies. In principle, therefore, the spatial distribution of galaxies encodes a wealth of information about the initial conditions for structure formation, gravitational evolution, the relationship (bias) between galaxies and mass, and the processes involved in galaxy formation. To extract this information, the statistical properties of the galaxy distribution must be measured and compared with the predictions of structure formation models.

To date, two-point statistics of the cosmic microwave background and the large scale structure, i.e., the two-point correlation function and its Fourier transform the power spectrum, have been the primary means of testing structure formation models. This is appropriate, since two-point statistics provide the lowest-order measures of departure from homogeneity; moreover, for Gaussian fluctuations, they provide a complete statistical description of the density field. However, to precisely probe structure formation models, it is necessary to go beyond second-order information, for: i) the observed galaxy distribution *is* non-Gaussian and, in particular, its web-like spatial coherence is not captured by two-point information; ii) the dissipative processes of galaxy formation in general imply that the galaxy distribution differs from the underlying dark matter field. This latter bias between galaxies

and mass (Kaiser 1984; Davis *et al.* 1985; Bardeen *et al.* 1986) is only partly constrained by two-point statistics.

Given these limitations of the two-point function, in this paper we consider higher order statistics of the galaxy distribution. The theory of higher order statistics is well-developed (e.g., Peebles 1980; Fry 1984; Bernardeau 1992, 1994; Juszkiewicz, Bouchet & Colombi 1993; Bouchet *et al.* 1993; Colombi, Bouchet & Schaeffer 1995; Szapudi *et al.* 1998; Colombi *et al.* 2000; Szapudi *et al.* 2000). In particular, it has been shown that higher order moments of the galaxy distribution provide important constraints on non-Gaussianity in the initial conditions (Fry & Scherrer 1994; Jaffe 1994; Chodorowski & Bouchet 1996; Gaztañaga & Mähönen 1996; Frieman & Gaztañaga 1999; Scoccimarro 2000; Feldman *et al.* 2001; Durrer *et al.* 2000) and on the bias (Fry & Gaztañaga 1993; Frieman & Gaztañaga 1994; Gaztañaga & Frieman 1994, Fry 1994; Juszkiewicz *et al.* 1995; Matarrese, Verde and Heavens 1997; Frieman & Gaztañaga 1999; Szapudi 1999; Scoccimarro *et al.* 2000; Feldman *et al.* 2001).

Here, we measure the  $s_p$  parameters (which characterize the connected moments of counts in cells, hereafter CIC) of the angular galaxy distribution in early SDSS data; these can be viewed as normalized area averages of the projected (angular)  $p$ -point correlation functions. We use the same data set for which second-order statistics were recently reported by Connolly *et al.* 2001, Dodelson *et al.* 2001, Scranton *et al.* 2001, Szalay *et al.* 2001, and Tegmark *et al.* 2001. Direct estimation of the angular and redshift-space three-point correlation functions in early SDSS data will be presented elsewhere.

Previous measurements of angular galaxy CIC include those obtained for the Automated Plate Measuring (APM, Gaztañaga 1994, Szapudi *et al.* 1995) and Edinburgh Durham Souther Galaxy Catalog (EDSGC, Szapudi, Meiksin, & Nichol 1996) surveys. Both have a wide area covering  $\sim 1$  steradian to  $b_J \sim 20$  and constructed from digitized UK Schmidt plates. Similar measurements were performed in the Deeprange catalog (Postman *et al.* 1998, Szapudi *et al.* 2000), based on a deeper ( $I < 23.5$ ), small-area (16 sq. deg.) CCD imaging survey. The SDSS sample considered here is intermediate between these two extremes in both area ( $\sim 160$  sq. deg) and depth ( $r < 22$ ). We note that all of these datasets contain of order  $10^6$  galaxies with measured angular positions and apparent magnitudes. While the SDSS dataset is based on only two nights of early imaging data and constitutes less than 2% of the eventual survey area, the high quality of the data has enabled us to extract statistical measurements with smaller errors than those for the earlier catalogs; the SDSS results therefore provide an important consistency check on and interpolation between the previous measurements. According to Colombi, Szapudi & Szalay (1998) the full SDSS will pinpoint the skewness and kurtosis with smaller than 1% and 10% errors, respectively, in a large dynamic range up to  $10h^{-1}\text{Mpc}$ .

The next Section briefly describes the SDSS data set used, while Section 3 presents an outline of the method used for analysis. Section 4 contains the measurements and various tests for systematic effects, while Section 5 is devoted to comparisons with measurements in other surveys. We present our conclusions in Section 6.

## 2. The Sloan Digital Sky Survey Early Data Set

The Sloan Digital Sky Survey is a wide-field photometric and spectroscopic survey being undertaken by the Astrophysical Research Consortium at Apache Point Observatory in New Mexico (York *et al.* 2000). The completed survey will cover approximately 10,000 square degrees. CCD imaging with the SDSS camera (Gunn *et al.* 1998) will include  $10^8$  galaxies in five passbands ( $u, g, r, i$ , and  $z$ ; see Fukugita *et al.* 1996) to an approximate detection limit of  $r = 23$  at signal-to-noise  $S/N = 5$  (strictly true for point sources).

In this paper, we focus on a small section of imaging data that was taken on the nights of March 20 and 21, 1999, during commissioning of the survey telescope; these data are designated Runs 752 and 756 and are in the Northern Equatorial Stripe of the survey. These interleaved scans are centered on the Celestial Equator, covering a stripe 2.52 deg wide, with declination  $|\delta| < 1.26^\circ$ , and approximately 90 deg long, with Right Ascension ranging from  $9^h 40^m 48^s$  to  $15^h 45^m 12^s$  (J2000). These data, designated EDR-P and discussed extensively by Scranton *et al.* (2001), constitute a high-quality subset of the data made publicly available as part of the SDSS Early Data Release (Stoughton *et al.* 2001).

The imaging data were reduced by the SDSS photometric image processing software (`photo`), which detects objects and measures their apparent magnitudes based on the best-fit PSF-convolved de Vaucouleurs or exponential model, including an arbitrary scale size and axis ratio. All magnitudes were corrected for Galactic extinction using the reddening maps of Schlegel, Finkbeiner, & Davis (1998). For this dataset, two methods of star-galaxy separation were available. The version of the photometric pipeline used to reduce these data makes a binary decision about whether a given detected object is stellar or galactic. For most of the results shown below, we selected all objects flagged as galaxies in this way by `photo`. While the `photo` separation works well at bright magnitudes, a Bayesian star-galaxy separation method (Scranton *et al.* 2001), which assigns a probability to each object of being a star or galaxy, provides a more precise separation at faint magnitudes. Below, we also show results for a sample of objects for which the Bayesian method assigns a very high probability ( $p > 0.99$ ) of their being galaxies. We find that these two samples yield consistent results for the higher order moments.

Observing conditions, particularly the seeing, varied considerably over the course of these two nights of data taking. Scranton *et al.* (2001) carried out extensive tests of the effects of seeing, galactic extinction, variable stellar density, etc., on the integrity of the data. These tests showed that the data were essentially free of systematic contamination (as demonstrated by cross-correlation analysis), provided certain regions were excluded, and we apply the same masks here. The resulting masks depend on apparent magnitude: a “bright” seeing mask (used for  $r < 21$ ) excludes regions where the seeing disk is larger than  $1.75''$ , while the “faint” seeing mask (used for  $21 < r < 22$ ) excludes regions for which the seeing exceeds  $1.6''$ . These masks exclude roughly 30% of the data area. In addition, regions where the reddening is greater than 0.2 mag in  $r$  and small rectangles around saturated stars and ghost images were also masked out. The resulting catalog contains  $1.46 \times 10^6$  galaxies in the apparent magnitude range  $18 < r < 22$  and covers an area of 160 (140) square degrees for the bright (faint) samples. The resulting data region has a complex geometry (see Figs. 13-14 in Scranton *et al.* 2001), complicating the CIC analysis, as described below. Since the data tests described in Scranton *et al.* (2001) were based solely on two-point analyses, the results shown below provide additional constraints on the data quality: the consistency of the  $s_p$  measurements with both previous results and theoretical predictions indicates that stellar and other contamination of the sample is small.

As in Connolly *et al.* 2001, Dodelson *et al.* 2001, Scranton *et al.* 2001, Szalay *et al.* 2001, and Tegmark *et al.* 2001, we divide the sample into four (‘de-reddened’) apparent magnitude slices,  $r = 18 - 19, 19 - 20, 20 - 21, 21 - 22$ . We also consider a “pseudo APM” slice, with  $r = 15.9 - 18.9$ , in order to compare with the results of Gaztañaga (2001a), as well as a series of slices with  $r = 17.9 - 18.9, 18.9 - 19.9, 19.9 - 20.9, 20.9 - 21.9$  for direct comparison with the results from the Deeprange survey (Postman *et al.* 1998, Szapudi *et al.* 2000).

### 3. The Counts in Cells Method

The probability distribution of counts in cells (CIC),  $P_N(\theta)$ , is the probability that an angular cell of (linear) dimension  $\theta$  contains  $N$  galaxies. The factorial moments of this distribution are defined by  $F_k \equiv \sum_N P_N(N)_k$ , where  $(N)_k = N(N-1)\dots(N-k+1)$  is the  $k$ -th falling factorial of  $N$ . The factorial moments are closely related to the moments of the underlying continuum random field (which is assumed Poisson-sampled by the galaxies),  $\rho = \langle N \rangle (1 + \delta)$ , through  $\langle (1 + \delta)^k \rangle = F_k / \langle N \rangle^k$  (Szapudi & Szalay 1993), where angle brackets in the last relation denote an area average over cells of size  $\theta$ . The factorial moments therefore provide a convenient way to estimate the angular connected moments,  $s_p \equiv \langle \delta^p \rangle_c / \langle \delta^2 \rangle^{p-1}$ , where the subscript  $c$  denotes the connected contribution, and  $\langle \delta^p \rangle_c$  denotes the area average

(over scale  $\theta$ ) of the  $p$ -point angular correlation function. The moments  $s_3$  (skewness) and  $s_4$  (kurtosis) quantify the lowest-order deviations of the angular distribution from a Gaussian.

To measure the  $s_p$  amplitudes from CIC via factorial moments, we must estimate the distribution of CIC in the survey. We use the infinite oversampling algorithm of Szapudi (1997), which eliminates measurement errors due to the finite number of sampling cells. From the factorial moments, the recursion relation of Szapudi & Szalay (1993) is used to obtain the  $s_p$ 's. This technique is described in more complete detail in Szapudi, Meiksin & Nichol (1996) and Szapudi *et al.* (2001).

The masks described in section 2 represent the most serious practical problem for CIC estimation, since they generate a complex geometry for the survey area. In addition to the seeing masks, there are a large number of small cut-out holes around bright stars, ghosts, etc., yielding about 20,000 separate mask regions. Since the cut-out holes are distributed across the entire survey area, a randomly placed cell larger than about  $0.1^\circ$  on a side has a high probability of intersecting a mask. In the standard CIC technique, cells that overlap mask regions are discarded, since one has no information about the galaxy field in the masked portion of the cell. In principle, this would limit our analysis to cells smaller than  $\simeq 0.1^\circ$ .

To remedy this situation, we follow Szapudi *et al.* (2001) and carry out the CIC analysis by ignoring all masks with area smaller than 0.0021 square degrees; this leaves only about 300 of the largest masks. Using only the large masks allows us to extend the measurements to cell sizes of order  $1^\circ$ . We test the validity of this prescription by comparing measurements of the  $s_p$  with all the masks and with only the large masks, for cells smaller than  $0.1^\circ$ . We find that we can reliably use just the large masks to make measurements on larger scales, since the discarded small masks occupy a falling fraction of the cell area as the cell size increases.

The errors on the  $s_p$  measurements shown in the figures were estimated by using the FORCE (Fortran for Cosmic Errors) package (Szapudi & Colombi 1996, Colombi, Szapudi, & Szalay 1998, Szapudi, Colombi & Bernardeau 1999). This method provides the most accurate estimation of the errors from the data itself and takes into account the contributions from the six (eight) point correlations to the errors on  $s_3$  ( $s_4$ ). It includes error contributions from finite-volume effects, edge effects, and discreteness. The FORCE-estimated errors depend on a number of parameters, several of which can be accurately estimated from the data itself (e.g., the mean cell occupation number, the angular two-point function averaged over the area of a cell, and the effective area of the survey). With one exception, the remaining parameters are obtained from models, e.g., Extended Perturbation Theory (Colombi *et al.* 1997) is used to estimate  $s_6$  and  $s_8$ ; as shown by Szapudi, Colombi & Bernardeau (1999), the  $s_p$  errors are relatively insensitive to variations of these model parameters within their

presently acceptable ranges. The final parameter needed is the estimate for the area-average of the two-point correlation function over the full survey region, which we have measured from 100  $\Lambda$ CDM realizations (including galaxy bias) obtained with the **PTHalos** code (Scoccimarro & Sheth 2001). These simulations of the galaxy distribution are generated by using second-order Lagrangian perturbation theory to follow clustering at large scales and to identify dark matter halos, which are then replaced by nonlinear dark matter profiles to build the small-scale correlations. Galaxy distributions are obtained by sampling the dark matter profiles with a number of galaxies that depends on the halo mass  $m$ , according to  $N_{\text{gal}}(m) \sim m^{0.8-0.9}$ . This galaxy-halo scaling leads to an approximate match between the measured angular two-point function in early SDSS data and the  $\Lambda$ CDM model; see Scranton *et al.* (2001) for a detailed description of this scaling relation and comparison of the **PTHalos** angular two-point correlation with measurements in the data.

We also use the **PTHalos** realizations to independently estimate  $s_p$  errors and their covariance matrix by averaging over the Monte Carlo pool. Due to the significant computational cost required to measure higher-order moments, however, we have only used this approach for the  $r = 18 - 19$  and 19-20 magnitude slices, which have the fewest galaxies. Directly comparing the **FORCE** and **PTHalos** errors in this case for both  $s_3$  and  $s_4$ , we found that they agree to better than 30%, with the **FORCE** errors being larger (smaller) than the **PTHalos** errors for angular scales larger (smaller) than 0.05 degrees. Given the different assumptions that go into the two methods, this consistency is quite encouraging; while the **FORCE** uses as input the measured higher order correlations and assumes the hierarchical model ( $s_p = \text{const.}$ , independent of  $\theta$ ), the **PTHalos** estimate is based on correlations built from  $\Lambda$ CDM models plus a bias prescription which does not necessarily lead to  $s_p = \text{const.}$  (see, e.g., the solid curves in Fig. 2 below). In addition, the elongated geometry of the survey region and the large number of masks present an extra challenge for the **FORCE** method; the agreement with the **PTHalos** estimates for the two bright slices indicates that the **FORCE** maintains accuracy under these conditions.

The **FORCE** error estimation is based on a series expansion: when the relative errors approach unity, it breaks down. When this occurs, the **FORCE** correctly indicates that the errors are qualitatively large, but the actual size of the errorbars has no precise statistical meaning in this regime. Finally, while the **FORCE** method is able to calculate the cosmic bias of the estimators of  $s_p$  (Hui & Gaztañaga 1999; Szapudi, Colombi & Bernardeau 1999), its effects are always negligible in the regime where the **FORCE** errors are accurate (i.e., smaller than  $\sim 100\%$ ); therefore we do not include a cosmic bias estimate.

It should be borne in mind that error estimation using the **FORCE** or the **PTHalos** mock catalogs each represent model-dependent statistical error calculations. This is unavoidable,

since the errors are determined in part by galaxy clustering over scales larger than the survey region, which we cannot directly measure. The accuracy of the error estimates is determined by the difference between the assumed model and the actual distribution. In addition, these estimates do not include possible systematic errors in the data; however, the tests described in Scranton *et al.* (2001), although only performed for two-point statistics, suggest the latter are not dominant over the scales we consider. The FORCE error estimates are easily obtained for faint magnitudes where the PTHalos estimates require costly computational resources due to the relatively large number of galaxies. On the other hand, the PTHalos method can deal trivially with complex masks and edge effects; in addition, it provides the covariance matrix of the errors, essential for testing models since measurements at different scales are correlated.

#### 4. Measurements of Counts in Cells Statistics

We have carried out a series of measurements of CIC statistics in the early SDSS angular clustering data. We first present our principal results for the normalized connected moments  $s_3$  and  $s_4$  and their estimated statistical errors. To ascertain the reliability of these results, we have performed a number of auxiliary measurements aimed at quantifying the possible level of systematic errors. The most important of these tests are discussed in Sec. 4.2.

##### 4.1. Principal Measurements

Figure 1 shows the main results of this paper, the measurement of the angular amplitudes  $s_3$  (triangles) and  $s_4$  (squares) in the early SDSS data in four apparent magnitude bins. The error estimates were made using the FORCE method, as described in Section 3. The open symbols show the results using all the masks of Scranton *et al.* (2001); as the Figure shows and as described in Section 3, these measurements cannot be extended to cells much larger than  $0.1^\circ$ . The solid symbols show the results when only the large masks are used; on scales smaller than  $0.1^\circ$ , these estimates are essentially identical to those obtained with all the masks. As argued in Section 3, this agreement indicates that the measurements on larger angular scales using only the large masks should be reliable; as a result, the measurements can be extended to scales as large as  $\simeq 1.5^\circ$ , about half the width of the data stripe. The exception to this argument is the measurement of  $s_3$  in the faintest bin,  $21 < r < 22$ : in this case, there appears to be a systematic discrepancy between the all-mask and large-mask measurements even on small scales. We have checked that this is not due to spurious objects which entered the catalog through use of the partial masks. All calculations were repeated

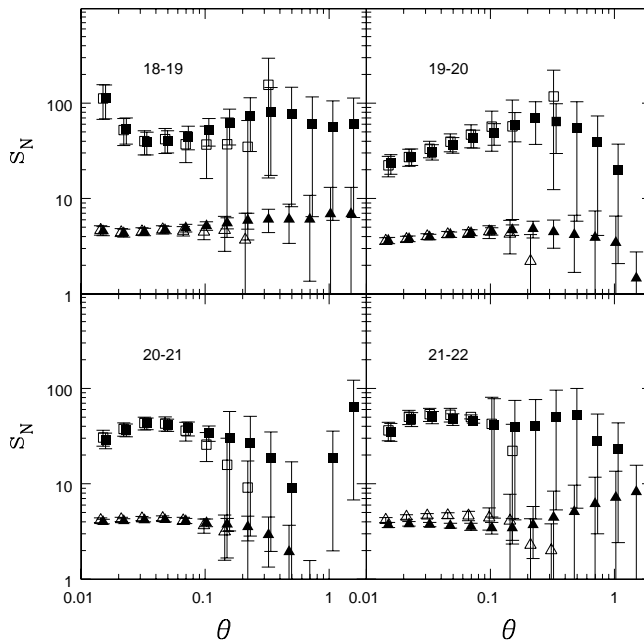


Fig. 1.— Results for the angular amplitudes  $s_3$  (triangles) and  $s_4$  (squares) in the early SDSS data set, in four bins of apparent magnitude ( $r$ ), with error estimates from the FORCE. Open (closed) symbols denote measurements with all masks (large masks only). For clarity, the points and errorbars have been shifted slightly between these two cases. For clarity, the largest relative errorbars plotted on the points are  $\sim 80\%$ , since the FORCE estimates are not numerically accurate when the errors are beyond this range.

with a catalog which was first filtered through the full bright and faint mask, respectively: partial masks on the filtered and unfiltered catalogs produce identical results.

To check the accuracy of the FORCE error estimates (in the presence of the complex masked geometry) and to compare the SDSS results with the predictions of structure formation models, we show in Figure 2 the results for  $s_3$  and  $s_4$  for the brightest flux slice,  $18 < r < 19$ , in eleven logarithmically spaced angular bins in the range  $0.01468^\circ - 1.6813^\circ$  (filled symbols, using the large masks). We also show the predictions based on 100 mock catalogs with a radial selection function chosen to match that of the data (Dodelson *et al.* 2001), based on the PTHalos code for a  $\Lambda$ CDM model (with  $\sigma_8 = 0.84$ ,  $\Omega_m = 0.3$ ,  $\Omega_\Lambda = 0.7$ ,  $\Gamma = 0.21$  at  $z = 0$ ) with ‘galaxies’ generated as briefly described in Section 3 (see Scranton *et al.* 2001 for details). The parameters of this model were chosen in order to reproduce the angular two-point function  $w(\theta)$  measured in the same SDSS data by Scranton *et al.* (2001) and Connolly *et al.* (2001). The solid curves show the mean of the 100 realizations, and the

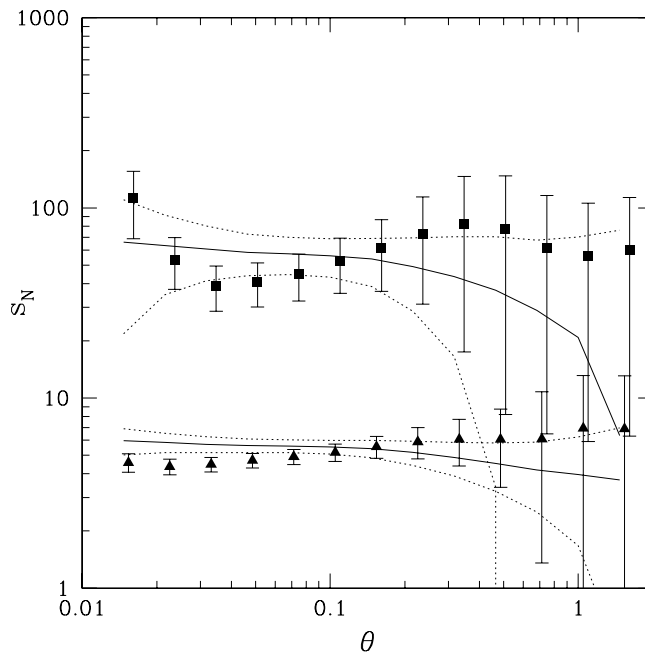


Fig. 2.— Results for  $s_3$  (triangles) and  $s_4$  (squares) for  $18 < r < 19$ , with FORCE errorbars. The solid curves show the mean results from 100 PTHalo simulations for  $\Lambda$ CDM, with the same survey geometry and selection function as the SDSS data. The dotted curves indicate the  $1 - \sigma$  deviations among the simulations.

dotted curves show the  $\pm 1\sigma$  deviations. The agreement between the variance estimates on  $s_3$  and  $s_4$  from FORCE and PTHalos is evident on scales  $0.03^\circ < \theta < 0.3^\circ$ . As noted above, on scales larger than  $\sim 0.3^\circ$ , where the relative errors are of order 100% of the value, or larger, the FORCE error estimates are not expected to be numerically accurate. On scales smaller than  $0.03^\circ$ , the mock catalogs predict somewhat higher variance than the FORCE. In any case, the overall agreement between these error estimates indicates the robustness of the results.

Figure 2 also indicates that the measured  $s_3$  and  $s_4$  amplitudes are in reasonably good agreement with predictions for galaxies in the biased  $\Lambda$ CDM model described above. To be more specific, we computed the goodness of fit of the  $\Lambda$ CDM model to the data using the full covariance matrix from the simulations; the resulting reduced  $\chi^2$  values are given in the second and third columns of Table 1. Given that this model was not explicitly constructed to give a good fit to  $s_3$  and  $s_4$ , it is in very good agreement with the data. We verified using mock catalogs that the Gaussian assumption for the likelihood function is a very good approximation on small scales, where most of the information is coming from.

In addition, we performed a fit of the SDSS results to a hierarchical model (HM), in which  $s_3$  and  $s_4$  are constrained to be constants, independent of cell size, again using the covariance matrix<sup>26</sup> from the PTHalos simulations<sup>27</sup>. The resulting higher order amplitudes and  $\chi^2$  values are shown in the fourth through seventh columns of Table 1. The relatively low reduced  $\chi^2$  values indicate that the resulting constant amplitudes provide a very good description of the data given the errors. Although there are apparent deviations from exact hierarchical scaling in Fig. 1, these are not statistically significant.

The high-quality CCD imaging in 5 passbands enables the SDSS to classify galaxies based on their photometric properties and therefore allows investigation of the clustering of galaxies as a function of galaxy type. As a first exercise at this, we have crudely divided the sample described above by morphological type: “ellipticals” designate objects for which the de Vaucouleurs profile fit is of higher likelihood than the exponential profile according to the `photo` pipeline, and “spirals” constitute the remainder. We have made no attempt to assess the reliability of this classification scheme as a function of magnitude or to correlate it with other photometric properties. The resulting  $s_p$  measurements for ellipticals (open symbols) and spirals (closed symbols) are shown in Figure 3. These results are suggestive: for example, the tendency for higher clustering amplitudes for the ellipticals, particularly on small scales, is at least qualitatively consistent with the well-known morphology-density relation. However, there is no clearly discernible trend in the results from bright to faint magnitudes, and the differences are for the most part not statistically significant given the errors on this relatively small sample. While we cannot draw firm conclusions from this first assay, it is evident that the full SDSS dataset should provide an excellent sample for studying higher order clustering as a function of galaxy type, especially if colors and spectral types are used in the selection (e.g., Iveic *et al.* 2001).

---

<sup>26</sup>Typically the cross-correlation coefficient between neighboring bins is larger than 0.9, and drops to 0.5 for angular scales separated by a factor of 4.

<sup>27</sup>For the faint magnitude slices,  $r = 20 - 21, 21 - 22$ , for which no explicit covariance matrix from PTHalos was available due to CPU limitations, we used the cross-correlation coefficient ( $r_{ij} \equiv C_{ij}/\sqrt{C_{ii}C_{jj}}$ ) from the  $r = 19 - 20$  catalogs and scaled up this matrix by the ratio of the diagonal ( $C_{ii}$ ) FORCE errors for the different simulation slices. This ansatz was tested by using it to scale from the  $18 - 19$  to the  $19 - 20$  slices, in which case it accurately reproduced the measured covariance matrix for the fainter slice. Here  $C_{ij}$  is the covariance matrix of the  $s_p$  estimator for cell sizes  $\theta_i$  and  $\theta_j$ .

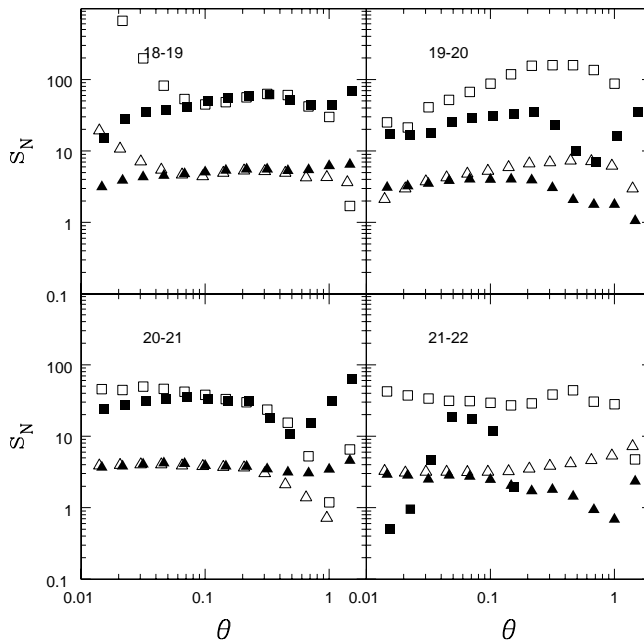


Fig. 3.—  $s_3$  and  $s_4$  measurements for “elliptical” (open symbols) and “spiral” galaxies (closed symbols) in early SDSS data. Only measurements with the large masks are shown, and errorbars are omitted for clarity. Objects in this sample were selected to have  $p_{gal} \geq 0.99$  according to the Bayesian star-galaxy separator (see Sec. 4.2).

#### 4.2. Auxiliary Measurements: Checks for Systematic Errors

We now describe a number of tests carried out in order to gauge possible systematic effects on the results. While the tests described by Scranton *et al.* (2000), although performed for two-point statistics, should imply the reliability of higher order statistics measurements, some extra checks are warranted.

In the results shown above, we used the SDSS image processing pipeline to perform star-galaxy separation: the resulting catalog contained all objects selected as galaxies by `photo`. As noted in Section 2, the Bayesian star-galaxy separation described in Scranton *et al.* (2001) provides a more accurate method at faint magnitudes, by assigning stellar and galactic probabilities to each object. To test the effects of possible stellar contamination of the `photo`-selected sample, we have repeated the  $s_p$  measurements using the Bayesian probabilities, by constructing a catalog containing all objects with galactic probability  $p_{gal} \geq 0.99$ . The results, shown in Figure 4, are almost indistinguishable from the `photo`-selected results of Figure 1. In the faintest magnitude slice, there appears to be a small difference in the results,

but it is not statistically significant. This test indicates that stellar contamination of the sample is not a significant source of systematic error in the measurement of  $s_3$  and  $s_4$ .

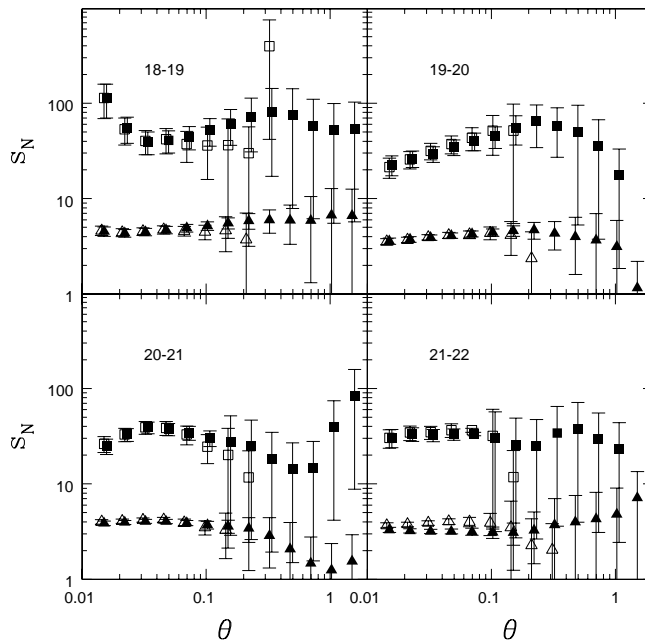


Fig. 4.— Same as Figure 1, but for a catalog containing galaxies selected with Bayesian probability  $p_{gal} \geq 0.99$ .

Another potential source of systematic error is incomplete masking of areas of poor-quality data, particularly bad seeing. The results shown above used the masks recommended by Scranton *et al.* (2001): the ‘bright’ mask (used for  $18 < r < 21$ ) excludes regions with seeing  $> 1.75''$ , and the more conservative ‘faint’ mask (used for  $21 < r < 22$ ) excludes regions where the seeing  $> 1.6''$ . Scranton *et al.* (2001) showed that these cuts yield a galaxy dataset with negligible cross-correlations with systematic effects such as stellar density, seeing, and dust extinction. As a further test, we have repeated the  $s_p$  estimates by excluding data with seeing  $> 1.6''$  in all four magnitude bins, i.e., applying the more stringent ‘faint’ seeing mask to the brighter ( $18 < r < 21$ ) data as well. The results are shown in Figure 5: solid symbols indicate the ‘bright’ seeing mask of  $1.75''$  and open symbols indicate results for the more conservative ‘faint’ seeing mask of  $1.6''$ . In both cases, we show results using only the large masks. There is evidence for small systematic shifts in the  $s_p$  amplitudes between the two masks, particularly for the two brightest slices; we speculate that the reduced effective survey area for the data with the ‘faint’ mask could lead to a small cosmic bias (a systematic underestimate) in the estimate of the  $s_p$ . However, the more important conclusion from this comparison is that almost all the changes are well within the  $1\text{-}\sigma$  errors, indicating that

systematic errors due to incomplete masking are well within the statistical errorbars. (Note that the  $s_p$  estimates at different  $\theta$  are correlated, so they cannot simply be combined to increase the significance of any differences.) To further test the effect of masks, we also computed the higher-order moments without using any mask at all. As shown in Figure 6, this results in an underestimate of  $s_3$  and  $s_4$  comparable to the differences seen in Figure 5. This should represent a conservative upper limit on possible systematic errors due to incorrect masking.

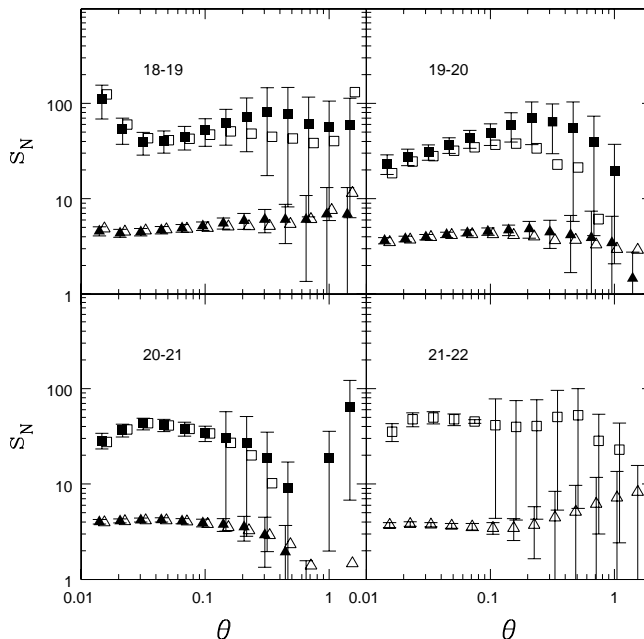


Fig. 5.—  $s_3$  and  $s_4$  measured with the Scranton *et al.* (2001) masks (solid symbols) compared with results using the more stringent 1.6'' ‘faint’ seeing mask for the three brightest flux slices (open symbols). The differences are well within the statistical errors. For clarity, errorbars are only plotted for the principal measurements.

As a further check, we have used the 100 PTHalos simulations of the  $18 < r < 19$  and  $19 < r < 20$  magnitude slices to check if the masks introduce any systematic errors into our measurements. We have performed three measurements in each mock SDSS catalog: (i) with no mask, (ii) with the ‘bright’ (large) masks, and (iii) with the ‘faint’ (large) masks, using the same CIC method as applied to the data. As expected, the errorbars were larger for the samples with more masked regions (smaller effective survey area), with the effect being more significant on large angular scales. On most scales, there is no systematic shift in the mean values of the  $s_p$  (no bias) between the 3 cases, although there is a slight bias toward lower  $s_p$  values on the very largest scales for the samples with more masked regions. As speculated

above, it is possible that an effective cosmic bias due to the skewness of the distributions of  $s_3$  and  $s_4$  values leads to a systematic underestimate of these amplitudes at large scales when the masked area is increased. We have attempted to quantify this effect from the mock catalogs, but the relatively small number of realizations (100) precludes us from reaching a definite conclusion. In any case, the amplitude of the bias of the  $s_p$  estimates is negligible compared to the measured variance. We conclude that no appreciable bias in the estimates of  $s_3$  and  $s_4$  can be attributed to the complicated geometry of the survey region.

## 5. Comparison with Previous Measurements

It is instructive to compare the early SDSS results for  $s_3$  and  $s_4$  with previous measurements. To compare with results from the APM and EDSGC surveys as well as with the early SDSS results reported by Gaztañaga (2001a), we have measured CIC statistics for SDSS galaxies in the 752/756 dataset with  $15.9 < r < 18.9$ . This choice is based on that of Gaztañaga (2001a), who demonstrated that the apparent magnitude range  $15.9 < g < 18.9$  in the SDSS yields a galaxy surface density comparable to the  $b_J < 20$  samples of the APM and EDSGC surveys. The  $r$ -selected sample used here will have a slightly different effective depth than his  $g$ -selected sample, but  $s_3$  and  $s_4$  should be relatively insensitive to this. A more substantive difference likely arises from the fact that samples selected in different passbands will contain different mixes of galaxy types and therefore yield different clustering amplitudes (see Figure 3); as a result, we do not expect these samples to yield identical higher order moments, but they should be qualitatively similar.

Figure 6 shows the results of this comparison for  $s_3$  (triangles and lower curves) and  $s_4$  (squares and upper curves) for the SDSS data with large masks (closed symbols with errors), the EDSGC measurement (solid curves, Szapudi, Meiksin, & Nichol 1996), and the APM survey (dotted curves, Gaztañaga 1994, Szapudi *et al.* 1995, Szapudi & Gaztañaga 1999). All measurements displayed here used the same CIC algorithm. The APM and EDSGC errorbars are omitted for clarity, since they are smaller than those for this bright SDSS sample which covers less area. On intermediate to large scales, the SDSS results are consistent at the  $1.5 \sigma$  level with both the APM and the EDSGC measurements. Going to small scales, the  $s_3$  amplitude in the SDSS appears to be intermediate between the EDSGC and APM values and remains fairly flat, while the latter two are rising and falling, respectively. This result is not too surprising: since the EDSGC and APM catalogs are based on digitized maps of essentially the same photographic plates, the differences between their results on small scales must be largely due to systematic effects in one or both of these catalogs. As noted by Szapudi & Gaztañaga 1999, the APM (EDSGC) amplitudes are likely biased low (high)

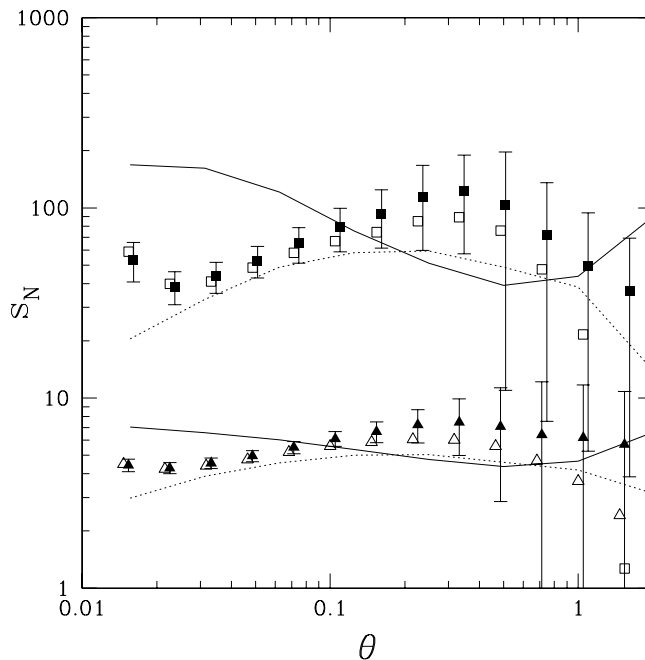


Fig. 6.—  $s_3$  and  $s_4$  measurements in the SDSS for  $15.9 < r < 18.9$  (closed symbols with FORCE errorbars) compared with results from the APM (dotted curves) and EDSGC (solid curves) surveys. Open symbols without error bars show the SDSS results when the masks are not used.

by their different methods of deblending objects in crowded fields. For the kurtosis,  $s_4$ , the SDSS results on small scales are also intermediate between the other two surveys, although somewhat closer to the APM values. Overall, the consistency between the measurements of the higher order moments in these different datasets is encouraging.

The results for  $s_3$  in the SDSS shown in Figure 6 appear to be in qualitative agreement with those obtained by Gaztañaga (2001a) on scales smaller than  $0.1^\circ$ , but they are systematically higher than his results on larger scales. There are several possible reasons for this discrepancy, and they may act in combination. The data in the survey region used in his analysis (Runs 94/125, Southern Equatorial Stripe), which does not overlap the region analyzed here, was taken for the most part in relatively poor seeing conditions early in the commissioning phase of the project. Application of the ‘bright’ seeing cut ( $1.75''$ ) recommended by Scranton *et al.* (2001) for the removal of systematic effects would mask out roughly 37% of the 94/125 area. Along with use of an undersampled CIC method, not including the masks could lead to an underestimate of  $s_3$  (Szapudi, Meiksin, & Nichol 1996; Szapudi & Gaztañaga 1998). As an example, the open symbols in Figure 6 show the results

for  $s_3$  and  $s_4$  for the 752/756 dataset when the ‘bright’ mask, which covers about 20 % of this data region, is not used. In addition to the mask, cosmic variance could also contribute to the difference in  $s_3$  results seen on large scales. Other small differences in the data selection between Gaztañaga 2001a and this paper ( $g$  vs.  $r$  selection, use of uncorrected vs. extinction-corrected magnitudes, use of Petrosian vs. model magnitudes) are probably less significant and unlikely to account for the difference in results. In fact, as we were about to submit this paper for publication, Gaztañaga 2001b appeared, which also included an analysis of  $s_3$  for the EDR north slice which we analyze in this paper. His results for this data slice are remarkably consistent with the open triangles in Figure 6, in which the mask is not used.

We turn next to comparison of the SDSS results with measurements in the Deeperange survey (Szapudi *et al.* 2000). The Deeperange catalog was selected in  $I$ ; for a typical galaxy SED, and assuming a mixture of early and late types, the approximate correspondence between SDSS  $r$  and  $I$  band is  $r_{sdss} \simeq I_{Deeperange} + 0.9$  (Postman 2001, private communication). We therefore constructed new SDSS samples in the  $r$  ranges 17.9–18.9, 18.9–19.9, ... to compare with the Deeperange samples of  $I = 17 - 18, 18 - 19, \dots$ . These SDSS samples are shifted by just 0.1 mag from those analyzed in Sec. 4. We note that the Deeperange magnitudes were not corrected for extinction, which should be negligible over this small, high-latitude field. The results of this comparison for  $s_3$  and  $s_4$  are shown in Figure 7, with solid symbols corresponding to the SDSS data and open symbols to the Deeperange. The figure panels are labeled by the Deeperange  $I$ -band range, e.g., I19 – 20 is compared with  $r = 19.9 - 20.9$  in the SDSS.

As expected, comparison of Figure 7 with Figure 1 shows that the 0.1 magnitude shift in the SDSS magnitude ranges causes very little change in the measured  $s_p$ ’s. The SDSS results for  $s_3$  are in excellent agreement with the Deeperange values in the three brightest slices, while the values are  $\simeq 1 - 2\sigma$  discrepant in the faintest SDSS slice. This suggests that the early SDSS data represents the most accurate measurement to date of the angular skewness for magnitudes  $r < 21$ . For  $s_4$ , there is also qualitatively good agreement between the two surveys for the 3 brighter magnitude slices, with a few discrepant points; this is not surprising, since the kurtosis is more sensitive to both systematic errors and cosmic variance than the skewness.

The comparison for the faintest SDSS slice  $r = 21 - 22$  is qualitatively different from the others: while the Deeperange data indicate a systematic falling off of the amplitudes with increasing sample depth, this trend is either absent or not significant in the SDSS data (see also Table 1). Given possible differences due to cosmic variance or undetected systematic errors, the current data cannot decide between these two trends. The answer, which has

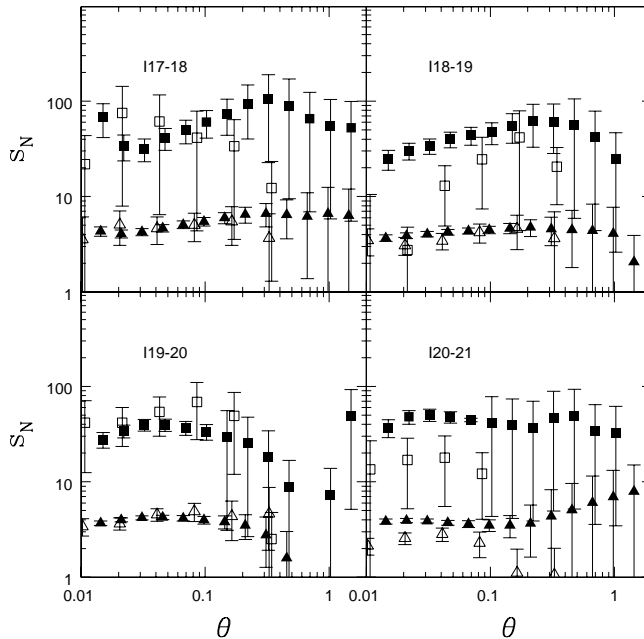


Fig. 7.—  $s_3$  and  $s_4$  for the Deeprange survey (open symbols), in  $I$  band magnitude slices 17 – 18, ..., 20 – 21, compared with SDSS results in the approximate corresponding  $r$  slices 17.9 – 18.9, ..., 20.9 – 21.9 (solid symbols). For each survey, the appropriate large masks were used, and the errorbars were calculated by the FORCE package.

important implications for the evolution of galaxy bias, should come when a larger SDSS sample is available.

## 6. Conclusion

We have measured the moments of angular counts in cells (CIC) in early SDSS data, using the Northern Equatorial Stripe. Although the results presented here focus on the higher order moments, we have also checked that the measured second order moments from CIC are consistent with the direct measurements of the angular two-point correlation function presented in Connolly *et al.* (2001) and Scranton *et al.* (2001). To control statistical and systematic errors, we have used state of the art measurement techniques and the highest quality segment of the available data. This resulted in a set of complicated masks, which probably does influence the accuracy of our measurement via edge effects. We have shown with auxiliary measurements and simulations that this should not produce any significant bias, only extra variance. According to Figure 4, star-galaxy separation has insignificant

contaminating effects on the  $s_p$  measurements, except perhaps for the faintest magnitude slice.

Figures 1-2 and Table 1 show that the  $s_p$ 's behave qualitatively as expected from theories of hierarchical structure formation. The  $s_3$  and  $s_4$  amplitudes display an approximate hierarchical scaling, with deviations consistent with cosmic (co)variance. As quantified in Table 1, the measurements of  $s_3$  and  $s_4$  are consistent with the predictions of non-linear  $\Lambda$ CDM models, in which the galaxy bias is determined by the fact that the number of galaxies in halos of mass  $m$  scales as  $N_{gal} \propto m^{0.8-0.9}$ . While this conclusion should be regarded as preliminary, given the limitations of the current data set and the restricted number of models considered, it is worth noting that a similar model matches the APM power spectrum and  $s_p$ 's on small scales (Scoccimarro *et al.* 2001).

We have also presented preliminary results for  $s_3$  and  $s_4$  for galaxies separated by morphological type into 'ellipticals' and 'spirals', based on profile fits to the images by the `photo` pipeline. As expected from the morphology-density relation, it appears that 'ellipticals' are more strongly clustered than 'spirals'; the robustness of this result remains to be demonstrated with a larger sample and a more refined method of morphological classification.

The Sloan Digital Sky Survey (SDSS) is a joint project of The University of Chicago, Fermilab, the Institute for Advanced Study, the Japan Participation Group, The Johns Hopkins University, the Max-Planck-Institute for Astronomy (MPIA), the Max-Planck-Institute for Astrophysics (MPA), New Mexico State University, Princeton University, the United States Naval Observatory, and the University of Washington. Apache Point Observatory, site of the SDSS telescopes, is operated by the Astrophysical Research Consortium (ARC).

Funding for the project has been provided by the Alfred P. Sloan Foundation, the SDSS member institutions, the National Aeronautics and Space Administration, the National Science Foundation, the U.S. Department of Energy, the Japanese Monbukagakusho, and the Max Planck Society. The SDSS Web site is <http://www.sdss.org/>. IS thanks Stephane Colombi for useful discussions and was partially supported by a NASA AISR, NAG-10750. We acknowledge the use of the FORCE (FORtran for Cosmic Errors) package by S. Colombi and IS, available from <http://www.ifa.hawaii.edu/~szapudi/istvan.html>.

## REFERENCES

- Connolly, A.J., *et al.* for the SDSS Collaboration 2001,ApJ, submitted, (astro-ph/0107417)  
Dodelson, S., *et al.* for the SDSS Collaboration 2001,ApJ, submitted, (astro-ph/0107418)  
23508

- Bardeen, J.R., Bond, J.R., Kaiser, N. & Szalay, A.S., 1986, *ApJ*, 304, 15
- Bernardeau, F. 1992, *ApJ*, 292, 1
- Bernardeau, F. 1994, *ApJ*, 433, 1
- Bouchet, F.R., Strauss, M.A., Davis, M., Fisher, K.B., Yahil, A., & Huchra, J.P. 1993, *ApJ*, 417, 36
- Chodorowski, M., Bouchet, F.R. 1996 *MNRAS*, 279, 557
- Colombi, S., Szapudi, I., Szalay, A.S., *MNRAS*, 296, 253
- Colombi, S., Szapudi, I., Jenkins, A., & Colberg, J., 2000, *MNRAS*, 313, 711
- Colombi, S., Bernardeau, F., Bouchet, F.R., & Hernquist, L. 1997, *MNRAS*, 287, 241
- Colombi, S., Bouchet, F.R., & Schaeffer, R. 1995, *A&A*, 281, 301 1780
- Davis, M., Efstathiou, G., Frenk, C. S., & White, S. D. M. 1985, *ApJ*, 292,371
- Durrer, R., Juszkiewicz, R., Kunz, M., Uzan, J-P. 2000, *Phys. Rev. D*, 62, 021301
- Feldman, H.A., Fry, J.N., & Frieman, J., Scoccimarro, R., 2001, *Phys. Rev. Lett.*, 86, 1434
- Frieman, J.A., Gaztañaga, E., 1994, *ApJ*, 425, 392
- Frieman, J.A., Gaztañaga, E., 1999, *ApJ*, 521, L83
- Fry, J.N. 1984, *ApJ*, 279, 499
- Fry, J.N. 1994, *Phys. Rev. Lett.*, 73, 215
- Fry, J. N., Gaztañaga, E. 1993, *ApJ*, 425, 1
- Fry, J.N., Scherrer, R.J. 1994, *ApJ*, 429, 36
- Gaztañaga, E. 1992, *ApJ*, 319, L17
- Gaztañaga, E. 1994, *MNRAS*, 268, 913
- Gaztañaga, E. 2001a, *astro-ph/0106379*
- Gaztañaga, E. 2001b, *astro-ph/01110126*
- Gaztañaga, E., Frieman, J. A. 1994, *ApJ*, 437, L13

- Hoyle, F., Szapudi, I., & Baugh, C.M. 1999, MNRAS, 317, 51
- Hui, L., Gaztañaga, E. 1999, ApJ, 519, 622
- Ivecic, Z. *et al.* for the SDSS Collaboration 2001, AJ, accepted
- Jaffe, A. H. 1994, Phys. Rev. D, 49, 3893
- Juszkiewicz, R., Bouchet, F. R., & Colombi, S. 1993, ApJ, 412, L9
- Juszkiewicz, R., Weinberg, D. H., Amsterdamski, P., Chodorowski, M., & Bouchet, F. 1995, ApJ, 442, 39
- Kaiser, N., 1984, ApJ, 273, L17
- Peebles, P.J.E. 1980, The Large Scale Structure of the Universe (Princeton: Princeton University Press)
- Postman, M., Lauer, T.R., Szapudi, I., & Oegerle, W. 1998, ApJ, 506, 33
- Scoccimarro, R. 2000, ApJ, 542, 1
- Scoccimarro, R., Feldman, H.A., Fry, J.N., & Frieman, J. 2000, ApJ, 546, 652
- Scoccimarro, R., Sheth, R., Hui, L., Jain, B. 2001, ApJ, 546, 20
- Scoccimarro, R., Sheth, R. 2001, (astro-ph/0106120)
- Scranton, R., *et al.* for the SDSS Collaboration 2001, ApJ, submitted, (astro-ph/0107416)
- Stoughton., C. *et al.* for the SDSS Collaboration 2001, ApJ, in prep.
- Szalay, A.S., *et al.* for the SDSS Collaboration 2001, ApJ, submitted, (astro-ph/0107419)
- Szapudi, I., & Gaztañaga, E. 1998, MNRAS, 300, 493
- Szapudi, I., Branchini, E., & Frenk C. 2000, MNRAS, 318, 45
- Szapudi, I., Colombi, S., Bernardeau, F., 1999, MNRAS, 310, 428
- Szapudi, I., & Colombi, S. 1996, ApJ, 470, 131 (SC96)
- Szapudi, I. & Szalay, A.S. 1993, ApJ, 408, 43
- Szapudi, I., Meiksin, A., & Nichol, R.C. 1996, ApJ, 473, 15
- Szapudi, I., 1997, ApJ, 497, 16

- Szapudi, I., Postman, M., Lauer, T.R., & Oegerle, W. 2001, *ApJ*, 548, 114
- Szapudi, I., Quinn, T., Stadel, J., & Lake, G., 1999, 517, 54
- Szapudi, I., Colombi, S., Jenkins, A., & Colberg, J., 2000, *MNRAS*, 313, 725
- Szapudi, I., Dalton, G., Efstathiou, G.P., & Szalay, A. 1995, *ApJ*, 444, 520
- Tegmark, M., *et al.* for the SDSS Collaboration 2001,*ApJ*, submitted, (astro-ph/0107418)
- York, D. *et al.* for the SDSS Collaboration 2000,*AJ*, 120, 1579
- Zehavi, I., *et al.* for the SDSS Collaboration 2001,*ApJ*, submitted, (astro-ph/0106476)

Table 1. The first two columns give the  $\chi^2$  per degree of freedom for the comparison of the SDSS data with the  $\Lambda$ CDM model. The remaining columns give the best-fit constant values for  $s_3$  and  $s_4$  (hierarchical model, HM) and their goodness of fit. All fits use the covariance of the measurements between different angular scales estimated from the mock catalogs.

$r$	$\chi^2_{\Lambda\text{CDM}}(s_3)$	$\chi^2_{\Lambda\text{CDM}}(s_4)$	$s_3^{\text{HM}}$	$\chi^2_{\text{HM}}(s_3)$	$s_4^{\text{HM}}$	$\chi^2_{\text{HM}}(s_4)$
18-19	1.4	1.4	$4.9 \pm 0.4$	0.7	$42 \pm 11$	1.2
19-20	1.8	1.6	$4.1 \pm 0.4$	0.8	$38 \pm 9$	1.1
20-21	—	—	$4.2 \pm 0.4$	0.7	$41 \pm 10$	0.7
21-22	—	—	$3.6 \pm 0.3$	0.8	$41 \pm 10$	0.7